Effect of Divergence on the Compressible Flow Patterns in Off-Design Planar Nozzles

San L. Tolentino

Research collaborator
Group of Mathematical Modeling and
Numerical Simulation (GMMNS)
Universidad Nacional de Ingeniería (UNI)
Lima
Perú

Jorge Mírez

Elec. Mech, Eng.; MSc & Dr Physics
Professor
Group of Mathematical Modeling and
Numerical Simulation (GMMNS)
Universidad Nacional de Ingeniería (UNI)
Lima
Perú

In the present work, the objective is to determine the Mach number and static pressure flow field behavior for off-design planar nozzle geometries with divergent angles of 1.21° (model A1) and 10.85° (model B1). ANSYS-Fluent R16.2 code was employed, and the RANS model and SAS turbulence model were applied to simulate in 2D the viscous flow field for the nozzle pressure ratio range of NPR 2.49 to 8.91. For model A1, in the divergent, the shock train is present, and the lateral pressure loads show fluctuations; in the centerline, the velocity is in the range of Mach 0.849 to 1.405. For model B1, the shock train is not present in the divergent, and the lateral pressure loads show flow separation; in the centerline, it is in the range of Mach 0.849 to 1.991. The flow velocity at the exit of the A1 model nozzle reaches Mach 1.357, which is 52.2% lower with respect to the B1 model, which has Mach 2.066. However, for the supersonic jet in the region of the atmosphere, the A1 model reaches Mach 2.967, which is 14.9% higher than with respect to the B1 model, which has Mach 2.522.

Keywords: *Compressible flow patterns, Flow velocity, Lateral pressure loads, Off-design planar nozzles, Shock train.*

1. INTRODUCTION

The compressible flow behavior and the aerodynamic profiles of the internal walls of supersonic nozzles applied to the aerospace area are recurrently studied. There are different geometrical configurations of mechanical devices that generate thrust, such as bell-shaped, parabolic, conical, planar, plug or aerospike full length or truncate, and expansion-deflection, among other geometries, [1-4]. It should be noted, typically, conical nozzle designs have the average divergent angle α in the range $12° \leq \alpha \leq 18°$, for which it performs well [1]. For divergent angles smaller than 12° are consi–dered off-design nozzles. The same design principle for conical nozzles applies to planar nozzles.

The investigation of the behavior of the comp–ressible flow field also extends to Ramjet and Scramjet jet engines [1,5,6], ducts [7,8], ejectors [9], diffusers [10,11], among other devices. As well as, it extends to the boundary layer theory [12], mathematical models of approximate solutions [13-15], solutions of analytical equations for isentropic flow that are impossible to invert by algebraic procedures [16-19], among others.

Depending on the nozzle pressure ratio (NPR) con–ditions, the flow can be overexpanded, adapted, or un–der-expanded [1,12]. For the overexpanded flow, shock waves occur in the divergent and in the atmosphere. Two schemes of the presence of shock waves for two geometrical configurations of the divergent are illus–trated in Fig. 1. As well as, Fig. 2 illustrates an image of the shock wave structure captured with the Schlieren

technique [20], which was reported by Verma and Manisankar [21].

The shock structure composed of the normal wave, oblique, and reflected waves interact with the turbulent velocity and thermal boundary layer of the flow region adjacent to the nozzle wall [12,22,23]. The structure of the shock waves is affected by the geometry of the inner wall curvature and the divergent angle, thus presenting different patterns of pressure side loads, flow separation modes, temperature changes, as well as, eddies, the res–tricted shock separation (RSS), and free shock separation (FSS) are present [12,24-28]. At the edges, such is the case of the edge at the end of the nozzle, Prandtl-Meyer expansion waves occur. The supersonic jet flow discharged to the atmosphere presents the plume shape, in which shock waveform structures are present [12,24].

Xue et al. [8] performed experimental tests on the motion of the shock train in the duct. The oscillation of separation position mainly characterizes shock train motion, while the separation shock strength is not so sensitive to downstream disturbance. Matsuo et al. [28] presented characteristics of shock train patterns in a duct. In the shock train region, the flow decelerates from supersonic velocity to subsonic velocity. Zhang et al. [29] studied the asymmetric structure of the oblique shock train for the flow in a duct. As well as Yuan et al. [30] studied the effect of inflow Mach numbers on shock train dynamics and turbulence features in a backpressure supersonic channel flow.

Mason et al. [31] performed experimental studies of the flow pressure at the walls of off-design planar nozzles. The convergent and nozzle throat contour significantly affects the flow behavior. The shock train is presented in this section for very narrow divergent angles.
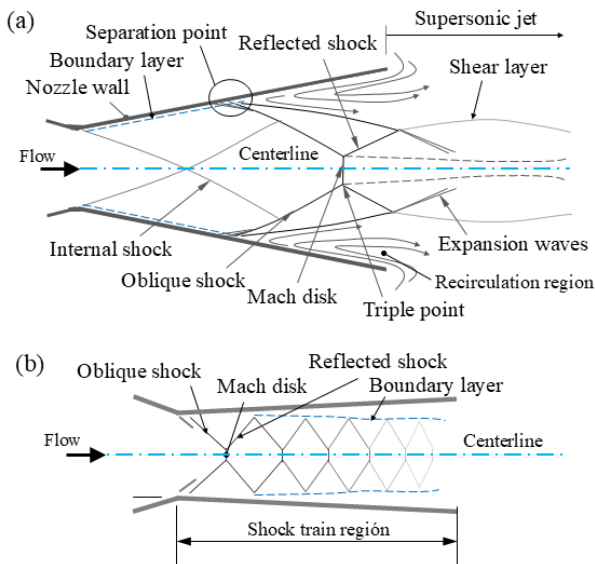
Figure 1. (a) Shock waveform structure for the overex–panded flow condition.(b) Structure of the shock train in the divergent.
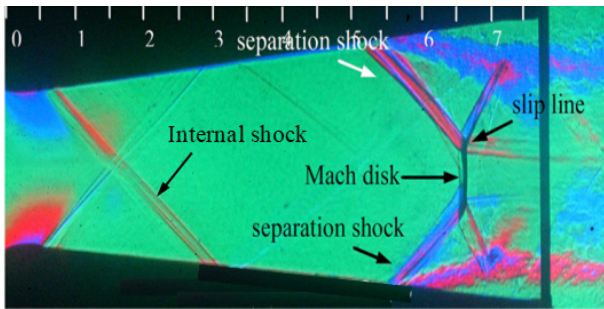
Figure 2. Shock waveform structure for flow in a planar nozzle [21].

Verma and Manisankar [21] performed experiments on an off-design planar nozzle and observed that the structure of the oblique and reflected waves presents an asymmetry, and in front of the shock front, a counter flow region is present. Tolentino et al. [27] performed computational simulations with computational fluid dynamics (CFD) tools for the flow field in an off-design planar nozzle. For increments of the divergent angle in the central region of the flow at the nozzle outlet, the flow velocity increases. Arora and Vaidyanathan [32] performed experiments for a planar nozzle with double divergent and reported that the angle of inflection affects the shock structure. Bourgoing and Reijasse [33] reported that wall roughness has an effect on the flow development of the flow in an off-design planar nozzle; they obtained different configurations of asymmetry of the shock wave structure. Hunter [34] performed experimental tests of flow separation in an off-design planar nozzle, indicating that the flow of the overexpanded nozzle was dominated by shock-induced boundary layer separation. Tolentino et al. [35] studied the flow behavior in off-design planar nozzles with straight-cut throats; as the throat length increases, the formation of oblique and reflected waves increases, and the flow velocity shows decelerations, which reaches a lower velocity at the end of the shock train.

Tolentino et al. [36] reported flow studies in off-design conical nozzles with straight-cut throats, where

the shock train evolves as the throat length increases. Roy and Ghosh [37] addressed the study of the shock train by Large-eddy simulation. Faheem et al. [38] addressed experimental studies for a set of nozzles emitting multiple supersonic jets. As the number of jets increases, the scattering rate decreases due to a decrease in drag; the cores of the supersonic jets are different from each other.

The present work has focused on continuing the research on cold air flow in planar nozzle geometries for models A1 and B1, as reported by Mason et al. The results of the work of Mason et al. [31] do not show images of the structure of the compressible flow field in the nozzle and in the atmosphere. In that sense, the si–mulation of viscous flow with CFD computational tools would provide approximate solutions of the flow field behavior, which would allow determining the distri–bution of Mach number and pressure gradients in the nozzle and in the atmosphere region, as well as identi–fying the regions of the flow where fluctuations occur.

The objective is to determine the Mach number flow field and static pressure behavior for two off-design planar nozzle geometries classified as models A1 and B1. The A1 model of the planar nozzle has a divergent half-angle $\alpha = 1.21°$, and model B1 has $\alpha = 10.85°$, be–ing both nozzles of equal geometries in the convergent and curvature of the throat, as well as its axial length. To simulate the turbulence of the viscous flow field for the NPR range 2.49 to 8.91, the ANSYS-Fluent R16.2 code [39] is employed. Section 2 presents the metho–dology. Section 3 presents the results and discussions. Section 4 presents the conclusions of the analysis.

2. MATERIALS AND METHODS

2.1 Experimental planar nozzle

The off-design planar nozzles classified as models A1 and B1, which are objects of study for viscous flow, are illustrated in Fig. 3. These nozzles have been used by Mason et al. [31] to measure the pressure of cold air flow for different NPRs in the range of 1.99 to 9.24. Pressure experiments for cold flow have been per–formed at the NASA Langley Research Center 16-Foot Transonic Tunnel Complex.

Table 1. Geometric parameters of the planar nozzles of models A1 and B1 [31]. Units are in centimeters (cm).

Parameter	A1	B1	Parameter	A1	B1
A_e(cm^2)	30.29	50.06	L_d (cm)	5.78	5.78
A_t(cm^2)	27.81	27.81	l_1 (cm)	5.54	5.54
A_e/A_t	1.09	1.80	l_2 (cm)	0.24	0.24
h_e (cm)	1.49	2.46	l_3 (cm)	0.01	0.13
h_i (cm)	3.52	3.52	l_4 (cm)	5.76	5.65
h_t (cm)	1.37	1.37	M_d	1.35	2.08
h_1 (cm)	1.41	1.41	NPR$_d$	2.97	8.81
h_2 (cm)	1.37	1.38	r_c (cm)	0.68	0.68
l (cm)	11.56	11.56	α (deg)	1.21	10.85
L_c (cm)	5.78	5.78	β (deg)	20.84	20.84

Model A1 (Fig. 3a) has been designed for Mach number $M_d = 1.35$, NPR$_d$ = 2.97, and area ratio A_e/A_t =

1.09. A_e is the area at the nozzle outlet, and A_t is the throat area. The divergent angle is α = 1.21°. Likewise, model B1 (Fig. 3b) has been designed for M_d = 2.08, NPR_d = 8.81, A_e/A_t= 1.8 and α = 10.85° [31]. A basic schematic of the planar nozzle is illustrated in Fig. 3c, in which the geometrical parameters are indicated. Table 1 presents the parameters of the geometrical dimensions, as well as including the aforementioned parameters.
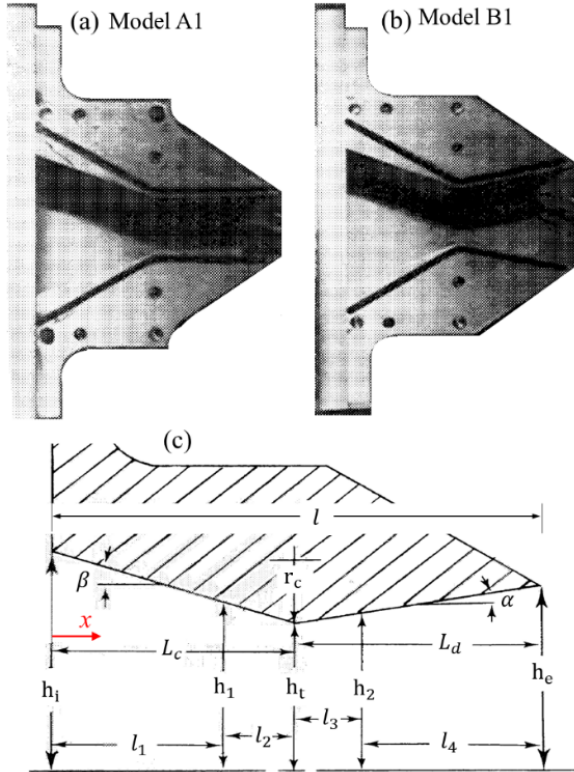

Figure 3. (a) Model A1 and (b) model B1 of the off-design planar nozzle. (c) Basic schematic of the planar nozzle geometry [31].

2.2 Computational domain

The spatial projection of the planar nozzle has been considered in 2D computational domains, and this is due to the symmetry of the nozzle. 2D domains are acceptable for symmetrical geometries since they save iterative computational time and decrease computational costs with respect to 3D domains. The 2D computa–tional domain was constructed with geometrical data presented in Table 1 [31]. The 2D computational do–main for model B1 is illustrated in Fig. 4, where the boundary conditions are applied, as well as the domain with structured mesh for grid 4 with 30736 quadrilateral cells. It should be noted that the computational domain and the meshing for model A1 are not presented in Fig. 4 since they are similar to model B1, the difference being that the divergence angle is smaller with respect to model B1.

The computational domain is parameterized for x/L_d, with the x direction being along the centerline and L_d being the divergent length. The nozzle section is in the range of $0 \leq x/L_d \leq 2$, and the atmosphere is in the range of $2 \leq x/L_d \leq 8$. It should be noted that the computational domain of the atmosphere section encompasses the discharge of the supersonic jet, the region where the

plume is present, so it is a section according to what is needed to simulate the turbulence of the flow.
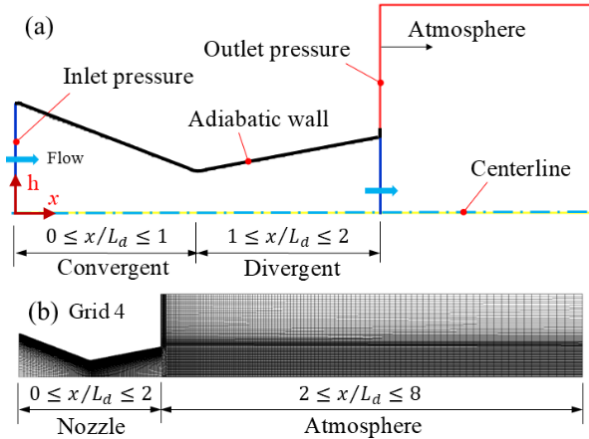

Figure 4. (a) 2D computational domain. (b) Structured grid 4 with 30763 quadrilateral cells.

The flow field is simulated for airflow, which is considered an ideal gas. The thermodynamic parameters of air are as follows: gas constant $R = 287$ J/(kg·K), specific heat ratio $k = 1,4$, specific heat at constant pressure $C_p = 1006,43$ J/(kg·K), and thermal conductivity k_t= 0,042 W/(m·K) [39].

The boundary conditions of cold flow pressure and temperature for seven cases of NPR for the planar no–zzle of model A1 and model B1 are presented in Table 2. The nozzle walls are considered adiabatic. The flow velocity at the wall is zero due to the no-slip condition. The flow velocity perpendicular to the centerline is zero. In the nozzle and in the atmosphere, the effect of gravity on the flow is not taken into account since they are considered 2D computational domains due to their symmetrical geometries. For the pressure at the inlet of the nozzle, $P_o = $ NPR·P, with $P = 101300$ Pa.

Table 2. Pressure and temperature parameters at the inlet and outlet of the planar nozzle.

Planar nozzle with α = 1.21° (model A1)	
Inlet pressure:	NPR: 2.49; 3.48; 4.47; 5.47; 6.45; 7.95 and 8.42
Inlet temperature:	$T_o = 300$ K
Outlet pressure:	$P = 101300$ Pa
Outlet temperature:	$T = 300$ K
Planar nozzle with α = 10.85° (model B1)	
Inlet pressure:	NPR: 2.94; 3.92; 4.88; 5.84; 6.81; 7.79 and 8.91
Inlet temperature:	$T_o = 300$ K
Outlet pressure:	$P = 101300$ Pa
Outlet temperature:	$T = 300$ K

2.3 Mathematical fundamentals

For the simulation of the viscous flow field in a transient state, the Reynolds-Averaged Navier-Stokes (RANS) equations are used. This model is efficient and suitable for simulations in 2D computational domains for compressible flow. The governing equations are the mass conservation equation, momentum, and energy [13,39].

The ideal gas equation of state [39] was used for the ideal gas flow condition. Shuterland's law equation [12] was used for the viscosity as a temperature function. The Scale-Adaptive Simulation (SAS) turbulence model [40] was used, which is coupled to the momentum equation of the RANS model.

For compressible flow, there are certain conside–rations for the Mach number: subsonic flow $0.3 \leq M \leq 0.8$, transonic flow $0.8 \leq M \leq 1.2$, supersonic flow $1.2 \leq M \leq 5$, hypersonic flow $M > 5$, and sonic flow $M = 1$. For incompressible flow, $M < 0.3$ is considered [41].

## 2.4 Computational solution method

The considerations taken into account in the ANSYS-Fluent R16.2 code [39], which applies the finite volume method (FVM) [13], are as follows. In Solver: density-based, transient, 2D space planar. Formulation: implicit. Flux type: Roe-FDS. Spatial discretization: least squares cell-based and second-order upwind. Transient formu–lation: second-order implicit. Residual monitor: 1×10^{-5} for continuity, energy, and k-omega. Surface monitors: mass flow rate. Convergence criterion: absolute. Solution initialization: hybrid. Time stepping method: fixed, and time step size (s): 1. Computational simu–lations of the flow field for the NPR range 2.49 to 8.91 were obtained in the range of 6000 to 21000 iterations.

2.5 Numerical convergence analysis

The computational domains for models A1 and B1 were meshed with quadrilateral cells in the ANSYS-Meshing platform and discretized using ICEM-CFD interaction. The mesh was refined for the flow region adjacent to the nozzle walls due to the presence of shear stresses. The numerical convergence study was taken into account for the B1 model due to the larger area of the divergent section and the atmosphere, which was meshed for four densities of quadrilateral cells, grid 1 with 19249 cells, grid 2 with 25658 cells, grid 3 with 27311 cells and grid 4 with 30736 cells. In the horizontal direction (x-axis), the convergent section is located in the range of $0 \leq x/L_d \leq 1$, the divergent in the range of $1 \leq x/L_d \leq 2$ and of the atmosphere in the range of $2 \leq x/L_d \leq 8$. It should be noted that the grid 4 mesh illustrated in Fig. 4b reported the following data: Minimum orthogonal quality: 0.0052034; orthogonal quality ranges from 0 to 1, where values close to 0 correspond to low quality. Maximum ortho skew: 0.98282; ortho skew ranges from 0 to 1, where values close to 1 correspond to low quality. Span angle center: fine. Smoothing: medium. Use advanced size function: curvature. Maximum aspect ratio: 232.598. For inflation: transition ratio 0.272; maximum layers: 2; and Growth rate: 1.2.

The computational domains of grids 1, 2, 3, and 4 were simulated for transient state flow with the SAS turbulence model [40] for NPR 8.91. As the grid density increases, the numerical values tend to converge; grid 4 is the one with the best stability in the Wall Y-plus (y^+) shear stress value (Fig. 5a), as well as for Wall shear stress (Fig. 5b), which were evaluated at the nozzle wall. The peaks of maximum Wall Y-plus and Wall shear stress values occur in the throat section at the

estimated position $x/L_d = 1$ (Fig. 5). For grid 4, the flow velocity at the outlet of the planar nozzle has the average Mach number of 2.066 and a percentage error of 0.816% with respect to the Mach number 2.083 for the isentropic Flow. As shown in Fig. 5a, the density of the grid cells is sensitive to the value of the shear stress; grid 4 has a cell density according to the geometry of the computational domain. It should be noted that a higher cell density greater than grid 4 is unnecessary, as it increases the computational cost for iterative compu–tation time, and the numerical results would be similar.
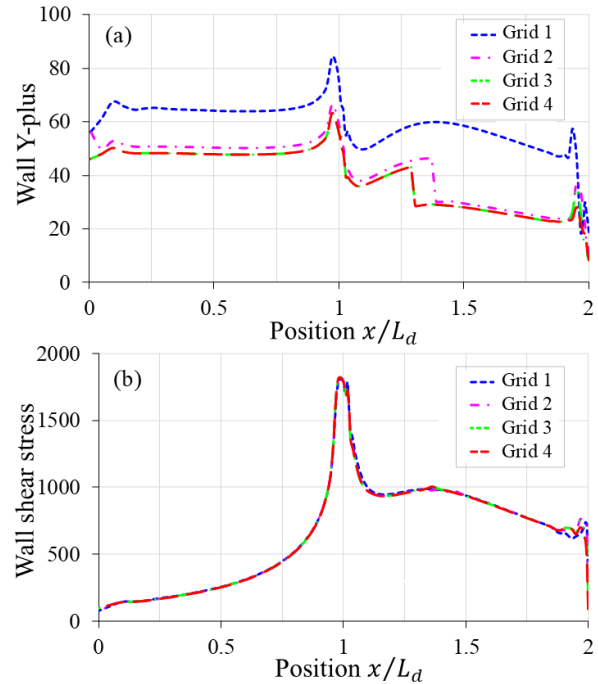
Figure 5. Profiles evaluated on the planar nozzle wall for NPR 8.91. (a) Wall Y-plus and (b) Wall shear stress.

The RANS (Reynolds-Averaged Navier-Stokes), URANS (Unsteady Reynolds-Averaged Navier-Stokes), DDES (Delayed Detached Eddy Simulation), and DNS (Direct Numerical Simulation) models have been reported in the literature. The RANS model is applied for a steady flow, averages turbulent fluctuations, and has a lower computational cost. The URANS model is applied for transient flow, takes vortex shedding phenomena into account, and is suitable for flows with moderate instabilities. The computational cost is higher than RANS. The DDES model is a hybrid between RANS and LES (Large Eddy Simulation) and is applied for transient flow; the results present a detailed resolution of complex turbulent structures, and the numerical results are more accurate than RANS and URANS and present a higher computational cost with respect to the two models mentioned above. DNS does not employ turbulence models, and the calculations involve 3D domains for the transient state solution of the Navier-Stokes equations. The results of the DNS model are more accurate, and the computational cost is extremely high with respect to the RANS, URANS, and DDES models that have been mentioned.

Due to the symmetry conditions that the 2D compu–tational domain of planar nozzles has, only SAS [40], DES SA [42], DES SST k-ω [43], and DES k- ω [44] turbulence models have been taken into consideration to

simulate the transient state flow for NPR 8.91, which were evaluated and compared with experimental pre–ssure data reported by Mason et al. [31] (Fig. 6). The curves of the pressure profiles evaluated at the nozzle wall are superimposed and intercepted with the experimental pressure data [31].

For a more rigorous analysis, the average Mach number at the nozzle outlet is considered as a control criterion, which should present percentage errors of less than 1% when compared to the Mach number for isentropic flow.

The best fit is presented for the SAS and DES SA models, which present the average Mach number of 2.066 at the nozzle outlet, with an error of 0.816% based on the isentropic flow for Mach number 2.083. While the other turbulence models present larger per–centages of errors. The DES SST k-ω model presents Mach 2.065 and an error of 0.864%, and the DES k-ε model presents Mach 2.064 and an error of 0.912%, respectively. For the computational simulations of the present work, the SAS model was chosen, and this is because the iterative computations for the numerical convergence are solved in less time with respect to the DES SA model.
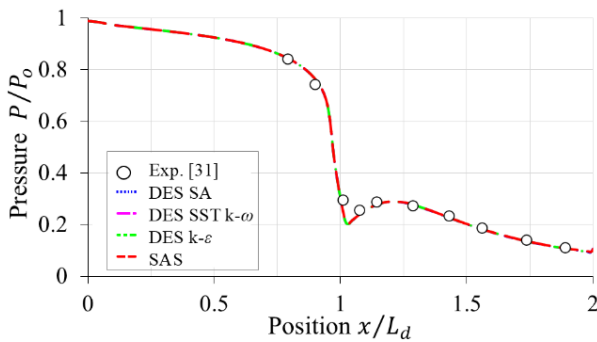

Figure 6. Pressure profiles were evaluated on the planar nozzle wall for grid 4 and NPR 8.91.

3. RESULTS AND DISCUSSION

In this section, the results obtained from the Mach num–ber flow field and static pressure for the planar nozzles

model A1 and model B1 are presented. The colored bars indicate lower magnitude values for the blue-colored regions and higher magnitude values for the red-colored regions.
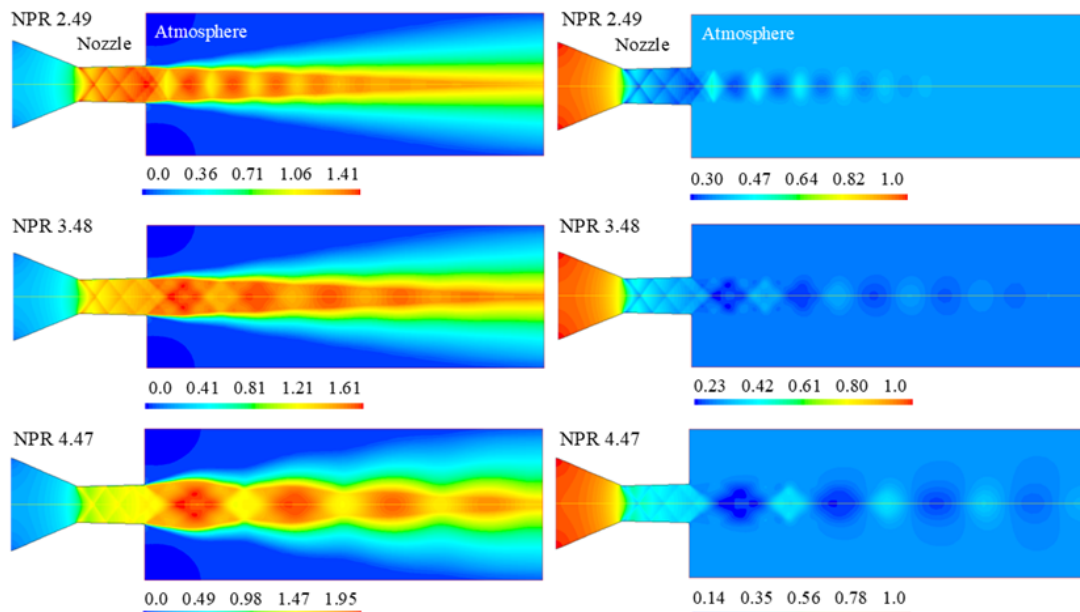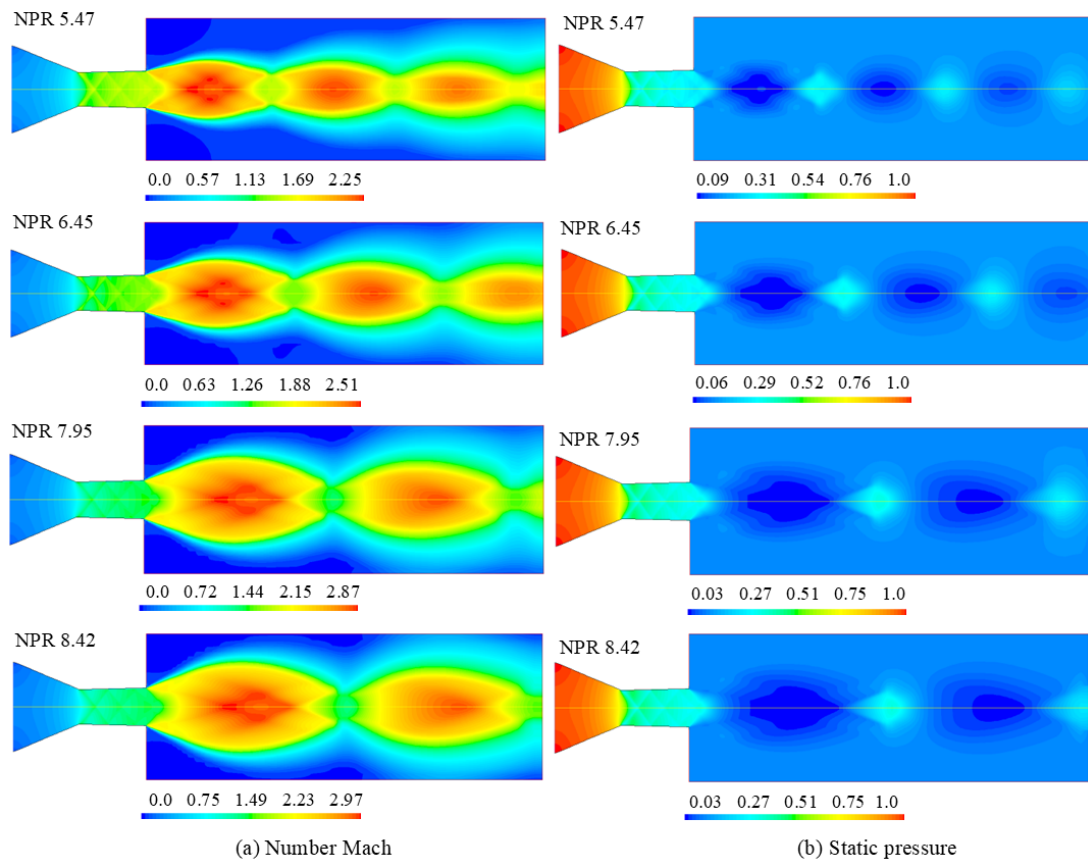
3.1 Planar nozzle model A1

The flow field in the planar nozzle model A1 with α = 1.21° for NPR values 2.49, 3.48, 4.47, 5.47, 6.45, 7.95, and 8.42 are shown in Fig. 7. For the Mach number it is illustrated in Fig. 7a and for the static pressure it is illustrated in Fig. 7b. The profiles evaluated at the centerline are illustrated for Mach number in Fig. 8a and for static pressure in Fig. 9a.

For NPR 2.49, the flow is overexpanded, and for values equal to or greater than NPR 3.48, the flow is under-expanded in the divergent ($1 \leq x/L_d \leq 2$) the flow presents velocity and pressure fluctuations, and the configuration of the shock train is observed which is composed of oblique and reflected waves, as well as the flow in certain regions is subsonic, transonic and supersonic.

In the centerline of the divergent ($1 \leq x/L_d \leq 2$) the behavior of the shock front as the flow oscillation propagates is observed. The shock front exhibits maximum and minimum velocity and minimum and maximum pressure.

It is observed in Fig. 8a and Fig. 9a that the first peak with the largest fluctuation occurs at the x/L_d = 1.2174 position with a velocity of Mach 1.399 and a pressure drop of $P/P_o = 0.3143$, as well as at position $x/L_d = 1.2663$ the flow decelerates to Mach 1.139 at the pressure of $P/P_o = 0.4457$. The second peak occurs at position $x/L_d = 1.5895$ with a velocity decrease of Mach 1.3681 and a pressure drop of $P/P_o = 0.3283$; as well at position $x/L_d = 1.6512$, the flow decelerates to Mach 1.2472, at a pressure of $P/P_o = 0.3871$. At the onset of divergence at $x/L_d = 1$, the flow reaches Mach 0.8492 and a pressure drop of $P/P_o = 0.6241$. As well as, at the nozzle exit at the $x/L_d = 2$ position, the flow velocity reaches Mach 1.4059 with a pressure drop of $P/P_o = 0.3113$.

(a) Number Mach   (b) Static pressure

Figure 7. Flow field patterns for planar nozzle model A1: (a) Mach number and (b) Static pressure.

Table 3 shows the positions and the maximum and minimum values of velocity and pressure fluctuation in the region of the shock train in the divergent centerline, as well as the values at the inlet and outlet of the divergent.

At the exit of the nozzle, we observe the behavior of the trajectories of the Mach number (Fig. 8b) and static pressure (Fig. 9b) profile curves that were evaluated in the direction and perpendicular to the centerline. The profiles have similar behaviors in the range of $0 \leq y/he \leq 0.8$. For the flow region adjacent to the nozzle wall, for the range of $0.8 \leq y/h_e \leq 1$, the NPR 2.49 departs from the other curves with lower Mach number values, while the pressure magnitude increases because of the velocity decrease due to flow braking.

For the flow at the nozzle outlet for NPR 2.49, the average values of Mach number are 1.149, and static pressure is $P/P_o = 0.4151$; whereas, for NPR 3.48 to 8.42, the Mach number is higher and static pressure is lower with respect to NPR 2.49. Table 4 shows the average values of Mach number and static pressure evaluated at the nozzle outlet.

It is observed for the supersonic jet discharge in the region of the atmosphere ($2 \leq x/L_d \leq 8$), as NPR incre–ases, the flow patterns exhibit oscillations (Fig. 7, Fig. 8, and Fig. 9). For NPR 2.49, the flow is overexpanded with Mach number fluctuations in the estimated range of $1 \leq M \leq 1.5$ and static pressure in the range of $0.3 \leq P/P_o \leq 0.55$. In the range of position $2 \leq x/L_d \leq 5$, the flow oscillates and is damped. In the range of position $5 \leq x/L_d \leq 8$ the flow has a tendency of slight fluctuations. For NPR 3.48, the flow oscillates around Mach number 1.5, and static pressure $P/P_o = 0.3$. The fluctuations

decrease for values equal to or greater than NPR 4.47 but with larger jumps in velocity and pressure, as presented for NPR 8.42, which reaches position $x/L_d = 3.236$, a maximum velocity of Mach number 2.967.
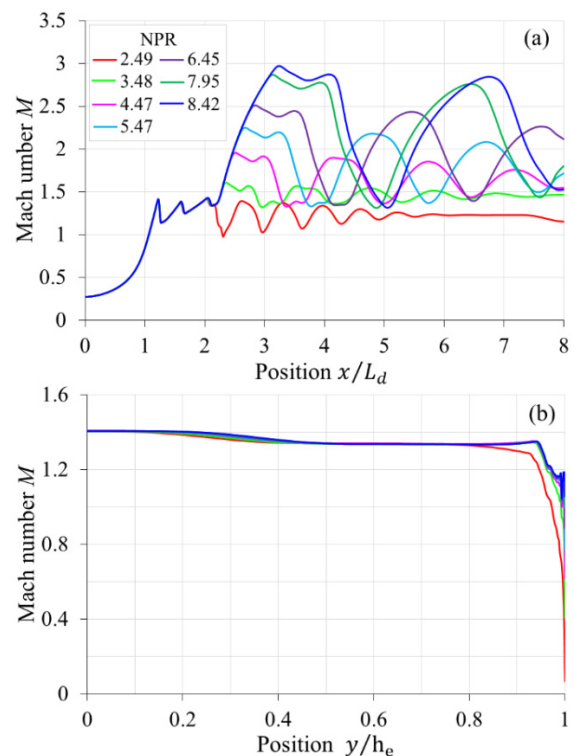
Figure 8. (a) Mach number profiles evaluated at the centerline. Position: convergent ($0 \leq x/L_d \leq 1$), divergent ($1 \leq x/L_d \leq 2$) and atmosphere ($2 \leq x/L_d \leq 8$). (b) Mach number profiles evaluated at the nozzle exit, at position $x/L_d = 2$.

It is observed that for divergent lengths $L_d = 5.78$ cm and $\alpha = 1.21°$, the flow behavior has a significant effect on the propagation of internal shocks, so the presence of the shock train is inevitable. The lateral pressure loads in the regions adjacent to the walls are not uniform but exhibit severe fluctuations resulting from changes in the amount of gas motion that compresses and decompresses as the flow moves toward the divergent outlet. As well, the velocity and pressure gradients interact with the central region of the flow, and the velocity and thermal boundary layer is affected in the regions of the flow adjacent to the walls.

Figure 10 illustrates the pressure patterns evaluated at the planar nozzle wall for NPR 2.49, 3.48, 4.47, 5.47, 6.45, 7.95, and 8.42, which are compared with experimental pressure data from the work of Mason et al. [31]. The profiles of the curve trajectories border the experimental data, following the trajectory of the variations of the lateral pressure loads. The flow is under-expanded for values equal to or greater than NPR 3.48; the flow at the nozzle outlet edge exhibits pressure drops.
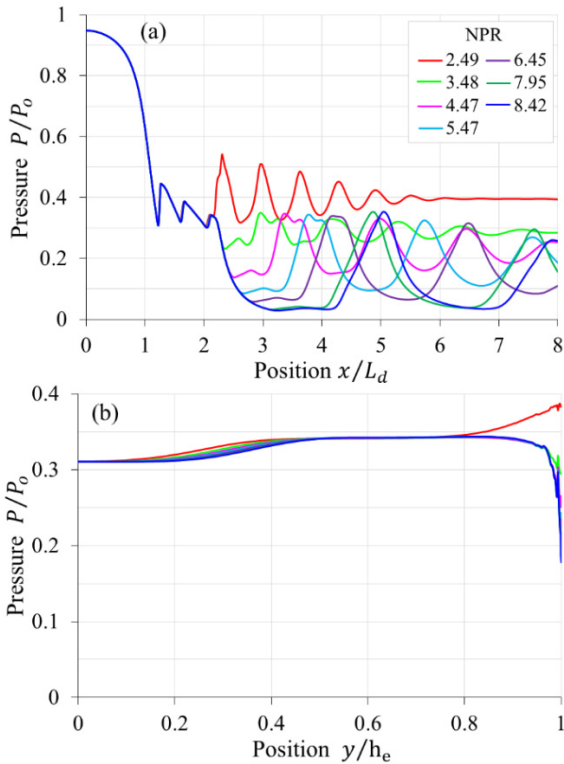
Figure 9. (a) Static pressure profiles evaluated at the centerline. Position: convergent ($0 \leq x/L_d \leq 1$), divergent ($1 \leq x/L_d \leq 2$) and atmosphere ($2 \leq x/L_d \leq 8$). (b) Static pressure profiles evaluated at the nozzle outlet, at position $x/L_d = 2$.

Table 3. Velocity and pressure fluctuations in the region of the shock train were evaluated in the divergent centerline ($1 \leq x/L_d \leq 2$).

Position x/L_d	Mach number	Static pressure
1	0.8492	0.6241
1.2174	1.3990	0.3143
1.2663	1.1390	0.4457
1.5895	1.3681	0.3283
1.6512	1.2472	0.3871
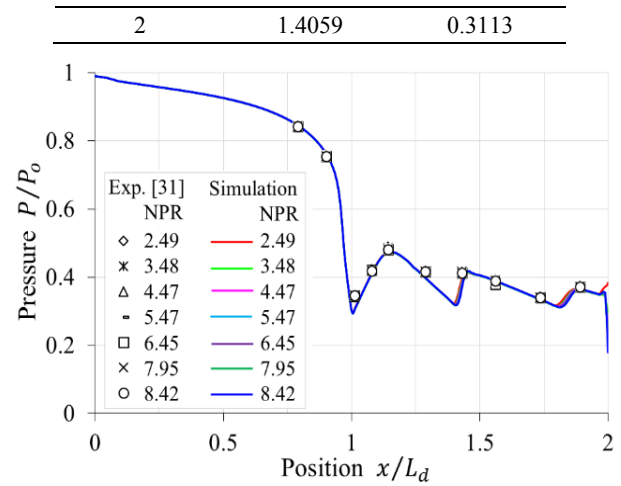
Figure 10. Comparison of the trajectories of the static pressure curves obtained at the planar nozzle wall of model A1 with experimental data from the work of Mason et al. [31].

Table 4. Average values of Mach number and static pressure at nozzle outlet, position $x/L_d = 2$.

NPR	Mach number (average)	Static pressure (average)
2.49	1.1490	0.4151
3.48	1.3287	0.3381
4.47	1.3481	0.3312
5.47	1.3526	0.3298
6.45	1.354	0.3293
7.95	1.3559	0.3289
8.42	1.3573	0.3285

3.2 Planar nozzle model B1

The flow field in the planar nozzle model B1 with $\alpha = 10.85°$ for NPR values 2.94, 3.92, 4.88, 5.84, 6.81, 7.79, and 8.91 are shown in Fig. 11. For the Mach number it is illustrated in Fig. 11a and for the static pressure it is illustrated in Fig. 11b. The profiles evaluated at the centerline are illustrated for Mach number in Fig. 12a and for static pressure in Fig. 13a.

For NPR 2.94, 3.92, 4.88, 5.84, 6.81, and 7.79, the flow is overexpanded, and for values equal to or greater than NPR 8.91, the flow is under-expanded. In the divergent ($1 \leq x/L_d \leq 2$), the flow presents velocity and pressure fluctuations, and internal shocks conformed by oblique and reflected waves are observed, where the flow in certain regions is subsonic, transonic, and supersonic.

Table 5 shows the positions and the maximum and minimum values of velocity and pressure fluctuation in the divergent centerline, as well as the values at the inlet and outlet of the divergent. Table 6 shows the average values of Mach number and static pressure evaluated at the nozzle outlet.

As shown in Fig. 12a and 12b, the maximum peak flow velocity occurs at the $x/L_d = 1.4867$ position for Mach 2.0133 with a pressure drop of $P/P_o = 0.1251$. At the $x/L_d = 1.6261$ position, the flow decelerates to Mach 1.8199 with a pressure drop of $P/P_o = 0.1687$. For NPR 2.94, the flow presents a normal shock wave front at the divergent, for supersonic flow at the $x/L_d = 1.8885$

position with Mach number 1.9255 and a pressure drop $P/P_o = 0.1433$ and, for subsonic flow at the $x/L_d =$

1.9352 position with Mach number 0.6162 and a pressure drop $P/P_o = 0.5927$.
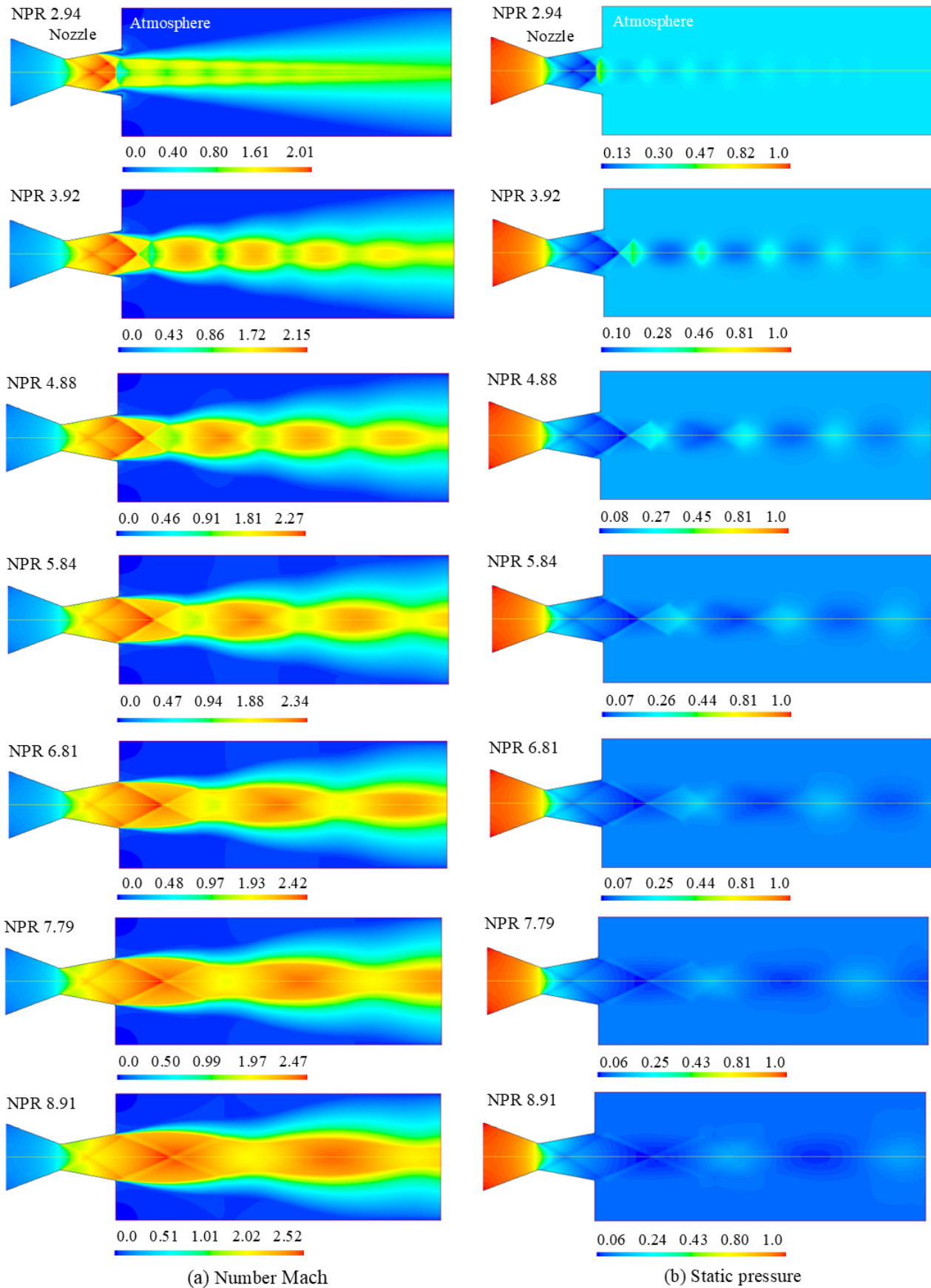

(a) Number Mach

(b) Static pressure

Figure 11. Flow field patterns for planar nozzle model B1: (a) Mach number and (b) Static pressure.

For the flow at the nozzle outlet (Fig. 12b and Fig. 13b), as the NPR increases, the curves' trajectories become agglomerated, achieving flow pattern stability for the under-expanded flow condition for NPR 8.91. It is noted that the flow is overexpanded for lower values of NPR 8.91. The average values (Table 6) for NPR 2.94, we have for Mach number 0.6437 with a pressure of $P/P_o = 0.4385$ and for NPR 8.91 Mach number 2.0661 with a pressure of 0.1132.

The curve trajectory for NPR 2.94 (Fig. 12b and Fig. 13b) shows that the flow velocities vary after the shock in different regions of the divergent. For the flow in the region adjacent to the wall in the range of $0.77 \leq y/h_e \leq 1$, a counter flow with adverse velocity and pressure gradients is present due to the presence of the oblique shock and inflow from the atmosphere. As the NPR increases, the oblique shock front wave moves toward the nozzle outlet (Fig. 11).

In the region of the atmosphere ($2 \leq x/L_d \leq 8$), the supersonic jet discharge exhibits damped fluctuations (Fig. 12a and Fig. 13a). For NPR 2.94 it oscillates in the estimated range of $0.6 \leq M \leq 1.25$ and of static pressure in the range of $0.29 \leq P/P_o \leq 0.59$. In the range of position $2 \leq x/L_d \leq 5$, the flow oscillates and is damped. In the range of position $5 \leq x/L_d \leq 8$, the flow fluctuations have a horizontal trend. The flow presents fluctuations with increasing and decreasing velocity for values equal to or greater than NPR 3.92. The flow for NPR 8.91 at position $x/L_d = 2.95$ reaches the maximum velocity of Mach number 2.522.

It is observed that the divergent length and angle $\alpha = 10.85°$ affect in the flow development with smaller fluctuations, where the internal shocks are composed of oblique and reflected waves.

The pressure patterns evaluated at the planar nozzle wall for NPR 2.94, 3.92, 4.88, 5.84, 6.81, 7.79, and 8.91 are shown in Fig. 14. which are compared with experimental pressure data from the work of Mason et al. [31]. The profiles of the curve trajectories border the experimental data, following the trajectory of the vari–ations of the pressure side loads. As the flow is over–expanded, flow separation occurs at the wall, so down–stream of the flow separation, the pressure increases. For NPR 8.91, the flow is under-expanded, so the pro–file follows a trajectory without pressure jumps up to the nozzle outlet.

Comparing the results of computational simulations of the compressible flow field of the planar nozzles model A1 with $\alpha = 1.21°$ and model B1 with $\alpha = 10.85°$, it is observed that the length and angle of the nozzle divergence have a significant effect on the flow regime. In the A1 model nozzle, the shock train is present with a higher presence of oblique and reflected waves, while in the B1 model nozzle, the presence of oblique and ref–lected waves is scarce. For the under-expanded flow at the nozzle outlet, model A1 for NPR 8.42 reaches the average value of Mach number 1.357 (Table 4) with an error of 0.52% with respect to the Mach number for isentropic flow. Meanwhile, the B1 model for NPR 8.91 reaches the average value of Mach number 2.066 (Table 6) with an error of 0.816%. The flow velocity at the nozzle outlet for model A1 is 52.2% lower with respect to the flow velocity of model B1.
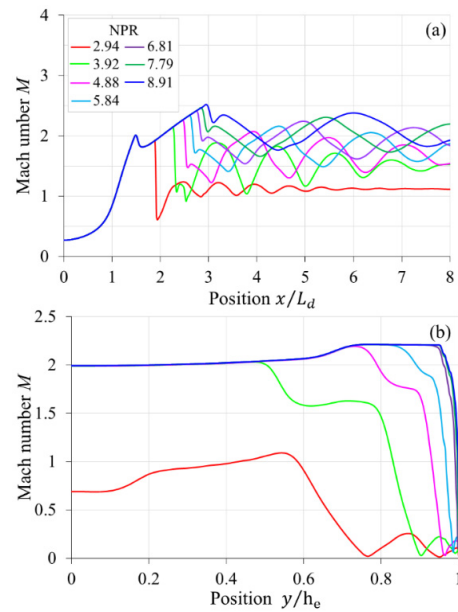
Figure 12. (a) Mach number profiles are evaluated at the centerline. (b) Mach number profiles evaluated at the nozzle exit, at position $x/L_d = 2$.

Table 5. Values of Mach number and static pressure fluctuations in the divergent centerline ($1 \leq x/L_d \leq 2$).

Position x/L_d	Mach number	Static pressure
1	0.8492	0.6241
1.4867	2.0133	0.1251
1.6261	1.8199	0.1687
2	1.9912	0.1294

Table 6. Average values of Mach number and static pressure at nozzle exit, position $x/L_d = 2$.

NPR	Mach number (average)	Static pressure (average)
2.94	0.6437	0.4385
3.92	1.5788	0.1776
4.88	1.8736	0.1332
5.84	1.9805	0.1208
6.81	2.0489	0.1147
7.79	2.0605	0.1137
8.91	2.0661	0.1132

The lower magnitude of the flow velocity at the exit of the A1 model nozzle is due to the fact that the flow fails to expand sufficiently in the divergent. However, at the centerline of the flow region in the atmosphere, the flow for NPR 8.42, at position $x/L_d = 3.236$, reaches a maximum velocity of Mach number 2.967. Meanwhile, the B1 model nozzle, at position $x/L_d = 2.95$, reaches a maximum velocity of Mach number 2.522, which is 14.9% lower with respect to the velocity of the A1 model flow.

The model A1 nozzle exhibits greater fluctuation of lateral pressure loads on the nozzle wall (Fig. 10) compared to the model B1 nozzle (Fig. 14). However, Model B1 has flow separation, and the flow separation point moves towards the nozzle outlet as the NPR increases.
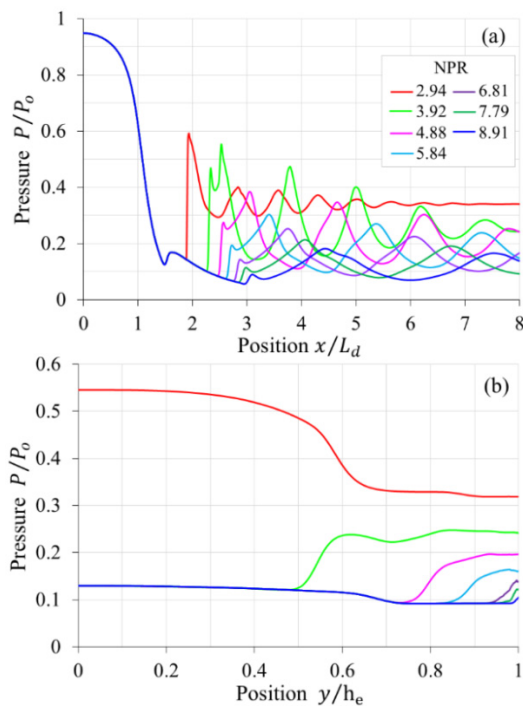
Figure 13. (a) Static pressure profiles evaluated at the centerline. (b) Static pressure profiles evaluated at the nozzle outlet, at position $x/L_d = 2$.
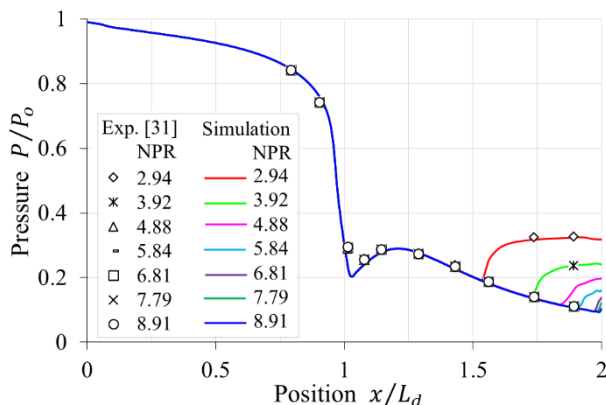
Figure 14. Comparison of the trajectories of the static pres–sure curves obtained at the planar nozzle wall of model B1 with experimental data from the paper of Mason et al. [31].

Results of the flow behavior in the divergent of the planar nozzle model A1 have different structures with respect to the shock train in nozzles with throat length. Such is the case of planar nozzles with $\alpha = 11.01°$[35], in the straight-cut throat the velocity fluctuations are in the range of Mach 1 to 1.2, and in Fig. 8a they are in the range of Mach 0.849 to 1.405. As well as, for the case of conical nozzles with $\alpha = 10°$ [36], in the straight-cut throat, the velocity fluctuations are in the range of Mach 0.6 to 1.8. Therefore, the Mach number range variations in the flow region where the shock train occurs are affected by the geometrical configurations of the nozzle walls. Also, for the case of the flow in the planar nozzle model B1, in Fig. 12a they are in the range of Mach 0.849 to 1.991. Similar results for overexpanded flow of the divergent shock structure in planar nozzles were reported in [21,27,34], as well as in conical nozzles [36, 45], where the oblique, reflected, and normal shock front are conditioned to the wall geometry and the divergent angle.

4. CONCLUSIONS

Based on the results of the compressible flow field in off-design planar nozzles for models A1 and B1 studied in the present work, the following conclusions were reached:

In the divergent of the planar nozzle model A1 with $\alpha = 1.21°$, the shock train is present. The flow velocity at the centerline is in the Mach number range from 0.849 to 1.405. At the nozzle exit, the under-expanded flow for NPR 8.42 reaches the average value of Mach number 1.357, which has an error of 0.52% with respect to isentropic flow. In the divergent wall, the lateral pressure loads show fluctuations due to the presence of the shock train. The flow in the region of the atmosphere reaches the maximum velocity of Mach 2.967.

With respect to the planar nozzle model B1 with $\alpha = 10.85°$, in the divergent, the presence of internal shocks is minimal, and the flow separation point moves toward the nozzle outlet as the NPR increases. At the centerline, the flow velocity is in the Mach number range of 0.849 to 1.991. At the nozzle exit, the under-expanded flow for NPR 8.91 reaches the average value of Mach number 2.066, which has an error of 0.816% with respect to isentropic flow. As well as the Mach number at the nozzle outlet for model A1 is 52.2% lower with respect to the flow velocity of model B1. In addition, for model B1, the flow in the atmosphere region reaches the maximum velocity of Mach number 2.522, which is 14.9% lower with respect to the flow velocity of model A1.

In future work, it is proposed to address studies of the shock train evolution in off-design planar nozzles for different divergent angles with increments of $\alpha = 1°$, for the range of $\alpha = 1°$ to $12°$.

REFERENCES

[1] Sutton, G.P. and Biblarz, O: *Rocket propulsion elements*, 9 ed., John Wiley and Sons, 2016.

[2] Scarlatella, G.,Tajmar, M. Bach, C.: Advanced nozzle concepts in retro-propulsion applications for reusable launch vehicle recovery: a case study, in:*72nd International Astronautical Congress (IAC),* Dubai, United Arab Emirates, October 25-29, 2021, https://iafastro.directory/iac/paper/id/65514/summary/

[3] Malina, F.J.: Characteristics of the rocket motor based on the theory of perfect gases, J. Frankling Inst., Vol. 230, No. 4, pp. 433-454, 1940, https://doi.org/10.1016/S0016-0032(40)91348-5

[4] Hagemann, G., Preusss, A., Grauer, F., Krestschmer, J. Frey, M., Ryden, R., Stark, R. andZerjeski, D.: Technology investigation for high area ratio nozzle concepts, in: *39th AIAA/ASME/SAE/ASEE Joint Propulsion Conference and Exhibit,* Hunstville, Alabama, 20-23 July 2003. https://arc.aiaa.org/doi/10.2514/6.2003-4912

[5] Li, M. et al.: Drag reduction characteristics of re–circulation flow at rocket base in an RBCC engine under ramjet/scramjet mode, Chinese Journal of Aeronautics, Vol. 37, No. 3, pp. 104-115, 2024. https://doi.org/10.1016/j.cja.2023. 11.021

[6] Zhao, G., Tian, Z., Pan, H., Shi, L. He, G.: Combustion mode and heat release characteristics of a kerosene-fueled rocket-aided ramjet combustor in ramjet-to-scramjet mode transition, Aerospace Science and Technology, Vol. 141, 108529, 2023. https://doi.org/10.1016/j.ast.2023.108529

[7] Sullins, G. and McLafferty, G.: Experimental results of shock trains in rectangular ducts, *AIAA fourth International Aerospace Planes Conference*, Orlando Fl., 1-4 December 1992, https://doi.org/10.2514/6.1992-5103

[8] Xue, L., Cheng, C., Wang, C., Zhang, L. Li, K. and Cheng, K.: Oblique shock train motion based on schlieren image processing, Chinese Journal of Aeronautics, Vol. 36, No. 3, pp. 30-41, 2023.https://doi.org/10.1016/j.cja.2022.10.013

[9] Elgezzar, M., Rashad, A., Hassan, M.S. Elnady, T.: CFD analysis and geometrical parameter investi–gation for the design of a high-efficiency super–sonic ejector, FME Transactions, Vol. 52, No. 1, pp. 1-11, 2024. https://doi.org/10.5937/fme2401 011E

[10] Bogar, T.J., Sajben, M. Kroutil, J.C.: Characteristic frequencies of transonic diffuser flow oscillations, AIAA Journal, Vol. 21, No. 9, pp. 1232-1240. https://doi.org/10.2514/3.8234

[11] Tolentino, S.L: Evaluation of turbulence models for the airflow in a transonic diffuser, Revista Politécnica, Vol. 45, No. 1, pp. 25-38. https://doi.org/10.33333/rp.vol45n1.03 (In Spanish)

[12] Schlichting, H., Gersten, K.:*Boundary-layer theory,* 9 ed., Springer-Verlag, Berlin Heidelberg, Ger–many, 2017.

[13] Ferziger, J.H., Perić, M. Street, R.L.:*Computational Methods for Fluid Dynamics*, 4 ed., Springer, Switzerland AG, 2020.

[14] Jemcov, A. Gonzales, J.P., Maruszewski, V., and Kelli, R.T.: Non-iterative wall model formula for non-equilibrium boundary layer flows, FME Transactions, Vol. 50, No. 2, pp. 223-237, 2022, https://doi.org/10.5937/fme2201223J

[15] Vujičić, M. and Crnojević, C.: Calculation of the turbulent flow in a plane diffuser by using the integral method, FME Transactions, Vol. 31, no. 2, pp. 69-74, 2003, https://www.mas.bg.ac.rs/_media/istrazivanje/fme/vol31/2/vujicic.pdf

[16] Abu-Irshaid, E.M.: *Asymptotic solutions for the fundamental isentropic relations in variable area duct flow*, Master´s thesis, University of Tennessee, Knoxville, 2006.

[17] Ferrari, A.: Exact solutions for quasi-one-dimensional compressible viscous flows in conical nozzles, Journal of Fluid Mechanics, Vol. 915, pp. 1-21, 2021. https://doi.org/10.1017/jfm.2020.1158

[18] Tolentino, S.L.: Empirical equation of the Mach number as a function of the stagnation pressure ratio for a quasi-one-dimensional compressible flow, FME Transactions, Vol. 51, No. 2, pp. 149-160, 2023. https://doi.org/10.5937/fme2302149T

[19] Tolentino, S.L: Comparative analysis of 2D simu–lations and isentropic equations for compressible flow in experimental nozzles, INCAS Bulletin, Vol. 15, No. 3, pp. 111-115, 2023. https://doi.org/10.13111/2066-8201.2023.15.3.9

[20] Krehl, P. and Engemann, S.: August Toepler - the first who visualized shock waves, ShockWaves, Vol. 5, No. 1, pp. 1–18, 1995. https://doi.org/10.1007/BF02425031

[21] Verma, S.B. Manisankar, C.: Origin of flow asym–metry in planar nozzles with separation, Shock Wa–ves, Vol. 24, No. 2, pp. 191–209, 2014. https://doi.org/10.1007/s00193-013-0492-1

[22] Bulat, P.V., Uskov, V.N.:Mach reflection of a shock wave from the symmetry axis of the supersonic nonisobaric jet. Research Journal of Applied Sciences, Engineering and Technology, Vol. 8, No. 1, pp.135–142, 2014. http://dx.doi.org/10.19026/rjaset.8.951

[23] Hadjadj, A., Ben-Nasr, O. Shadloo, M. S. Chaud–huri, A.: Effect of wall temperature in supersonic turbulent boundary layers: A numerical study, International Journal of Heat and Mass Transfer, Vol. 81, pp. 426-438, 2015. https://doi.org/10.1016/j.ijheatmasstransfer.2014.10.025

[24] Östlund, J., Muhammed-Klingmann, B.: Supersonic flow separation with application to rocket engine nozzles, ASME, Applied Mechanics Reviews, Vol. 58, No. 3, pp. 143–177, 2005. https://doi.org/10.1115/1.1894402

[25] Živković, S., Milinović, M., Adamec, N.: Expe–rimental and numerical research of a supersonic planar thrust vectoring nozzle via mechanical tabs, FME Transactions, Vol. 42, No. 3, pp. 205-211, 2014. https://doi.org/10.5937/fmet 1403205Z

[26] Zmijanović, V. Rašuo, B. Chpoun, A.: Flow sepa–ration modes and side phenomena in an overex–panded nozzle, FME Transactions, Vol. 40, No. 3, pp. 111-118, 2012, https://www.mas.bg.ac.rs/_media/istrazivanje/fme/vol40/3/03_vzmijanovic.pdf

[27] Tolentino, S.L. Mírez, J., González, O.: Numerical analysis of the Flow field in a planar nozzle for different divergent angles, JMES, Vol. 16, No. 4, pp. 9241-9252, 2022. https://doi.org/10.15282/jmes.16.4.2022.07.0731

[28] Matsuo, K. Miyazato, Y., Kim, H.D.: Shock train and pseudo-shock phenomena in internal gas flows, Progress in Aerospace Sciences, Vol. 35, No. 1, pp. 33-100, 1999, https://doi.org/10.1016 /s0376-0421 (98)00011-6.

[29] Zhang, Z., Cheng, C., Zhang, L.: Asymmetry of oblique shock train and flow control. Proceedings of the Institution of Mechanical Engineers, Part G: Journal of Aerospace Engineering, Vol. 238, No. 4, pp. 427-438, 2024. https://doi.org/10.1177/09544100241232160

[30] Yuan, T.F., Zhang, P.J., Liao, Z.M. and Wan, Z.H.: Effects of inflow Mach numbers on shock train dynamics and turbulence features in a back pressured supersonic channel flow, Physics of Fluids, Vol. 36, No. 2, 026126, 2024. https://doi.org/10.1063/5.0187688

[31] Mason, M.L., Putnam, L.E., Re, R.J.: The effect of throat contouring on two-dimensional converging-diverging nozzles at static conditions. NASA Technical Paper 1704, pp. 1-67, 1980. https://ntrs.nasa.gov/api/citations/19800020749/downloads/19800020749.pdf

[32] Arora, R., Vaidyanathan, A.: Experimental investi–gation of flow through planar double divergent nozzles, Acta Astronautica. Vol. 112, pp. 200-216, 2015.https://doi.org/10.1016/j.actaastro.2015.03.020

[33] Bourgoing, A., Reijasse, P.: Experimental analysis of unsteady separated flows in a supersonic planar nozzle, Shock Waves, Vol. 14, No. 4, pp. 251–258, 2005.https://doi.org/10.1007/s00193-005-0269-2

[34] Hunter, C.A.: Experimental investigation of sepa–rated nozzle flows, Journal of Propulsion and Po–wer, Vol. 20, No. 3, pp. 527-532, 2004. https://doi.org/10.2514/1.4612

[35] Tolentino, S.L., Mírez, J., Caraballo, S.A.: Nume–rical analysis of the shock train evolution in planar nozzles with throat length, FME Transactions, Vol. 51, No. 4, pp. 595-605, 2023. https://doi.org/10.5937/fme2304595T

[36] Tolentino, S.L., Mírez, J., Caraballo, S.A.: Nume–rical analysis of the shock train in conical nozzles with straight-cut throats, FME Transaction, Vol. 52, No. 2, pp. 186-195, 2024. https://doi.org/10.5937/fme2402186T

[37] Roy, A., Ghosh, S.: Large-eddy simulation of shock train in convergent-divergent nozzles with isoth-ermal walls, Journal of Turbulence, Vol. 25, No. 9, pp. 318-341, 2024. https://doi.org/10.1080/14685248.2024.2388314

[38] Faheem, M. et al.: Experimental study on the mean flow characteristics of a supersonic multiple jet configuration, Aerospace Science and Technology, Vol. 108, 106377, 2021. https://doi.org/10.1016/j.ast.2020.106377

[39] ANSYS-Fluent: Ansys Fluent Theory guide 2020R1.

[40] Menter, F., Egorov, Y.: The Scale-Adaptive Simu–lation Method for Unsteady Turbulent Flow Pre-dictions. Part 1: Theory and Model Description. Journal Flow Turbulence and Combustion, Vol. 85, pp. 113–138, 2010.https://doi.org/10.1007/s10494-010-9265-4

[41] White, F.: Fluids Mechanics, McGraw-Hill, Edu-cation, New York, 2016.

[42] Spalart, P., Deck, S., Shur, M.L., Squires, K.D., Strelets, M.K. and Travin, A.: A new version of detached eddy simulation, resistant to ambiguous grid densities, Theoretical and Computational Fluid Dynamics, Vol. 20, No. 3, pp. 181–195, 2006.https://doi.org/10.1007/s00162-006-0015-0

[43] Menter, F.R., Kuntz, M. and Langtry, R.: Ten Years of Experience with the SST Turbulence Model. Proceedings of the 4th International Symposium on Turbulence, Heat and Mass Transfer 4, Begell House Inc., West Redding, 2003. https://www.yumpu.com/en/document/view/16455902/ten-years-of-industrial-experience-with-the-sst-turbulence-model

[44] Shih, T.H, Liou, W.W., Shabbir, A., Yang, Z. Zhu, J.: A New k-ε eddy-viscosity model for high Reynolds number turbulent flows-Model develop–ment and validation, Computers Fluids, Vol. 24, No. 3, pp. 227–238, 1995. https://doi.org/10.1016/0045-7930(94)00032-T

[45] Tolentino, S.L., J. Mírez, J.: Throat length effect on the flow patterns in off-design conical nozzles, FME Transactions, Vol. 50, No.2, pp. 271-282, 2022, https://doi.org/10.5937/fme2201271T

NOMENCLATURE

A_e	Nozzle-exit area
A_t	Nozzle-throat area
A_e/A_t	Nozzle expansion ratio
L_c	Convergent section length
L_d	Divergent section length
M_d	Design, Mach number for isentropic flow
M	Mach number
P	Static pressure
P_o	Stagnation pressure
P/P_o	Ratio of static and stagnation pressures
T	Static temperature
T_o	Stagnation temperature
x/L_d	Distance/length ratio, nozzle divergent
y/h_e	Height/distance ratio, nozzle outlet
y^+	y-plus in shear stress value
α	Half-angle of the divergent section
β	Half-angle of the convergent section
CFD	Computational fluid dynamics
FVM	Finite volume method
FSS	Free shock separation
NPR	Nozzle pressure ratio
NPR_d	Design, Nozzle pressure ratio
RANS	Reynolds-Averaged Navier-Stokes
RSS	Restricted shock separation

ЕФЕКАТ ДИВЕРГЕНЦИЈЕ НА КОМПРЕСИБИЛНЕ ОБРАСЦЕ ПРОТОКА У РАВНИМ МЛАЗНИЦАМА ВАН ДИЗАЈНА

С.Л. Толентино, Х. Мирес

У овом раду, циљ је да се одреди Махов број и понашање поља статичког притиска за непро–јектоване планарне геометрије млазница са дивер–гентним угловима од 1,21° (модел А1) и 10,85° (мо–дел Б1). Употребљен је АНСИС-Флуент Р16.2 код, а примењени су РАНС модел и САС модел турбу–ленције да се симулира у 2Д поље вискозног струјања за опсег односа притиска млазнице од НПР 2,49 до 8,91. За модел А1, у дивергентном, ударни воз је присутан, а бочна оптерећења притиска показују

флуктуације; на средишњој линији, брзина је у опсегу од 0,849 до 1,405 маха. За модел Б1, ударни воз није присутан у дивергентном, а бочна оптерећења притиска показују раздвајање протока; на средишњој линији, налази се у опсегу од 0,849 до 1,991 маха. Брзина протока на излазу из млазнице модела А1 достиже 1,357 Маха, што је за 52,2% ниже у односу на модел Б1, који има 2,066 Маха. Међутим, за суперсонични млаз у области атмосфере, модел А1 достиже 2,967 маха, што је за 14,9% више него у односу на модел Б1, који има 2,522 маха.